

# contents

Supplementary Material .....	2
1. Computed tomography enterography protocol .....	2
2. Automatic segmentation of regions of interests .....	2
3. Radiomics feature extraction and selection .....	3
Supplementary Tables .....	4
Supplementary Table 1. Imaging features related to disease progression .....	4
Supplementary Table. 2 .....	7
Supplementary Table. 3 .....	7
Supplementary Table. 4 .....	8
Supplementary Table. 5 .....	11
Supplementary Table. 6 .....	12
Supplementary Table. 7 .....	13
Supplementary Table. 8 .....	16
Supplementary Figures .....	17
Supplementary Figure 1. ....	17
Supplementary Figure 2. ....	18
Supplementary Figure 3. ....	19

## Supplementary Material

### 1. Computed tomography enterography protocol

All patients with Crohn's disease were required to fast and ingest an oral polyethylene glycol electrolyte solution for six to eight hours, followed by ingestion of 1600–2000 mL of a 2.5% mannitol solution one hour before image acquisition. In the routine clinical scan, plain and dual phase contrast-enhanced CTs were performed from the dome of the liver to the symphysis pubis using one of the following CT scanners: Aquilion Vision (Canon Medical System, Otawara, Japan), Aquilion Prime (Canon Medical System), Somatom Force (Siemens Healthineers, Erlangen, Germany), GE Discovery CT 750 HD (GE Healthcare, USA), or Philips Brilliance iCT (Royal Philips Electronics, Amsterdam, Netherlands). The scanning parameters of the CT scanners are shown in the following table. After the plain scanning, 2 mL/kg of a non-ionic contrast agent was injected intravenously in the right antecubital vein at a rate of 3.5 mL/s using a dual-head power injector. The upper limit of the contrast dose was set at 150 mL for every patient. Forty millilitres of 0.9% saline was administered immediately after the injection of contrast agent at the same rate. The arterial phase scan was started 28 seconds post-injection, and the venous phase scan was initiated 70 seconds post-injection. In our study, plain CT enterography images were used for radiomics analysis.

**The scanning parameters of the five computed tomography scanners**

CT scanners	Aquilion Vision	Aquilion Prime	Somatom Force	GE Discovery CT 750 HD	Philips Brilliance iCT
<b>Hospital</b>	Center 1	Center 1	Center 1	Center 2	Center 3
<b>Scanner No.</b>	1	2	3	4	5
<b>Scanning parameters</b>					
Tube voltage, kVp	120	120	150	120	120
Tube current, mA	103	100	115	120	143
Pitch	0.813	0.637	0.6	0.984	0.984
Slice thickness, mm	1	1	1	0.625	5
Reconstruction interval, mm	0.8	0.8	0.7	0.625	5
<b>Contrast agent</b>	Ultravist 370	Ultravist 370	Ioversol 350	Ultravist 300	Iohexol 350

Centre 1, The First Affiliated Hospital of Sun Yat-Sen University; Centre 2, The First Affiliated Hospital of Shantou University Medical College; Centre 3, The First People's Hospital of Foshan City

### 2. Automatic segmentation of regions of interests

Based on the Python programming environment and the PyTorch deep learning framework, the nnU-Net<sup>1</sup> network structure, which can efficiently parse the semantic information of medical images was used to train an automatic segmentation model for visceral adipose tissue and subcutaneous adipose tissue. The training set, including 15 samples with fine delineation results, was from the training cohort. The Dice similarity coefficients of the segmentation of visceral adipose tissue and subcutaneous adipose tissue reached 0.90 and 0.93, respectively, which means that the performance of automatic segmentation was excellent. Visceral adipose tissue and subcutaneous adipose tissue were segmented automatically by using this model for the remaining of samples in the training cohort and total test cohort.

1 Isensee F, Petersen J, Klein A, et al. nnu-net: Self-adapting framework for u-net-based medical image segmentation. *arXiv preprint arXiv:180910486* 2018.

### 3. Radiomics feature extraction and selection

Briefly, extracted texture features included 14 shape-based features, describing the three-dimensional size and shape of the volume of interest; 18 first order statistics, describing the distribution of voxel intensity in the image area defined by the mask through common and basic metrics; 24 Grey Level Co-occurrence Matrix features (GLCM), describing how often a voxel occurs either horizontally, vertically, or diagonally to adjacent voxels with similar grey-level value (e.g., Contrast or Correlation); 16 Grey Level Run Length Matrix features (GLRLM), describing how many voxels with a given grey-level value occur in a sequence in the given direction (e.g., Short Run Emphasis or Long Run Emphasis); 16 Grey Level Size Zone Matrix features (GLSZM), describing how many voxels with a given grey-level value are connected (e.g., Small Area Emphasis or Large Area Emphasis); 14 Grey Level Dependence Matrix features (GLDM), describing the number of connected voxels within a given distance depending on the centre voxel (e.g., Small Dependence Emphasis or Large Dependence Emphasis); 5 Neighbourhood Grey Tone Difference Matrix features (NGTDM), describing the difference between a voxel and the average grey-level value of its neighbours (e.g., Coarseness or Busyness); 744 features for filter ‘Wavelet’ wavelet; and 279 features for filter ‘LoG’.

The two-step procedure for feature selection is as follows. First, those features with ICCs  $\geq 0.8$  remained. Then, we used the least absolute shrinkage and selection operator (LASSO) of the logistic regression algorithm to determine the best subset of radiomics features and reduce the likelihood of overfitting. LASSO is a linear model with an added regularisation term that tends to estimate sparse solutions, leading to fewer non-zero coefficients and effective feature reduction.

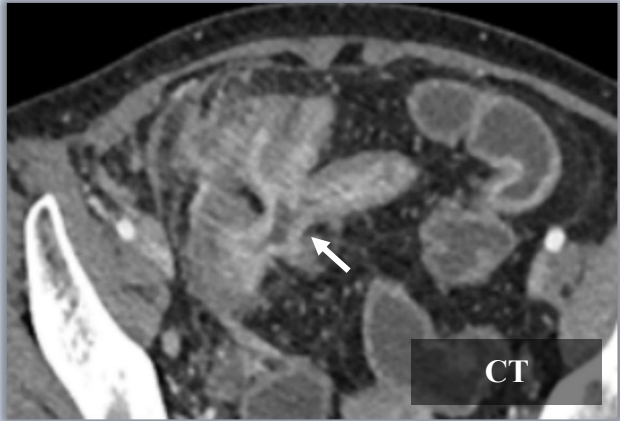
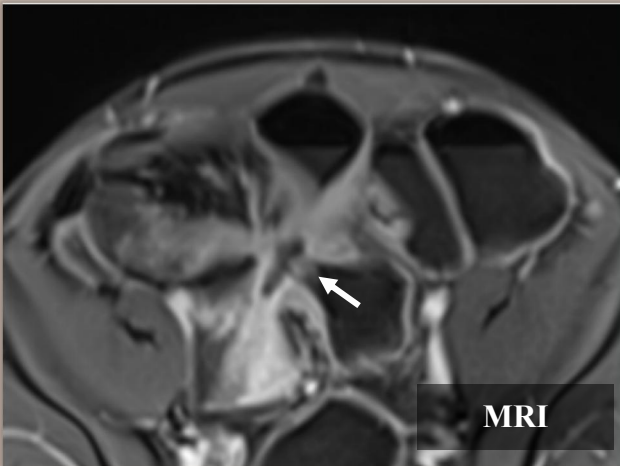
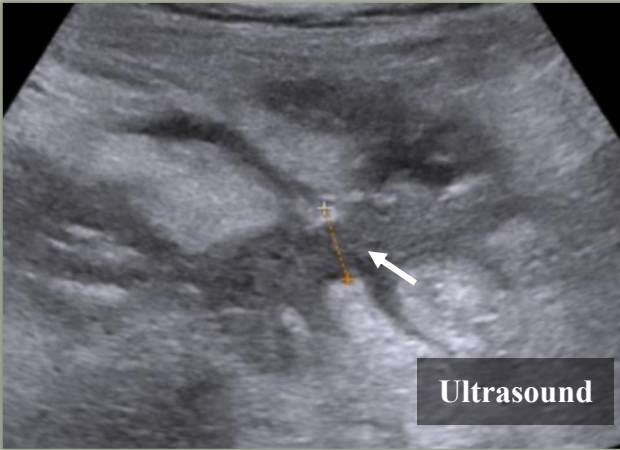
Mathematically, the objective function to minimise the loss in LASSO is:

$$Loss = \min \frac{1}{2n} \|y - X\omega\|_2^2 + \lambda \|\omega\|_1$$

LASSO aims to achieve the minimisation of the least squares penalty between the ground truth and predicted outcomes with added regularisation term  $\lambda \|\omega\|_1$ , where  $\lambda$  is a tuning weight constant and  $\|\omega\|_1$  is the L1-norm of the coefficient vector. Thus, the  $\lambda$  parameter decides the degree of sparsity of the coefficients, and it could be determined by cross validation based on minimum mean square error criteria. For cross-validation, we used leave-one-out cross-validation with the LASSO algorithm implemented by the LassoCV class in the Python module (scikit-learn, version 0.22; <https://www.scikit-learn.org/>). Finally, for the visceral adipose tissue radiomics model, the optimal  $\lambda$  value of 0.003 with  $\log(\lambda) = -2.523$  was selected in the LASSO logistic regression model, resulting in 36 radiomics features with non-zero coefficients. For the subcutaneous adipose tissue radiomics model, the optimal  $\lambda$  value of 0.004 with  $\log(\lambda) = -2.398$  was selected in the LASSO logistic regression model, resulting in 35 radiomics features with non-zero coefficients.

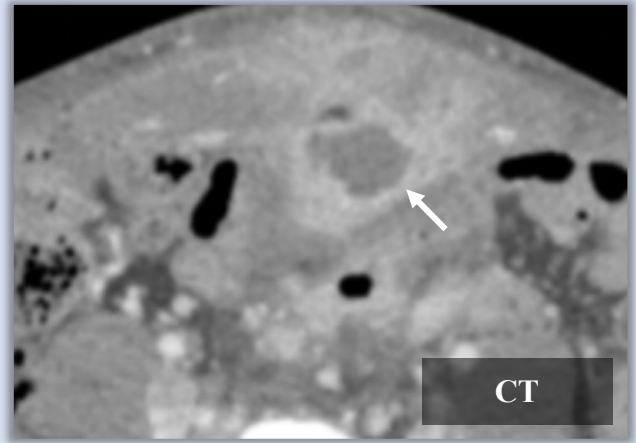
## Supplementary Tables

Supplementary Table 1. Imaging features related to disease progression

Penetrating disease <sup>1</sup> (Bowel fistula)	Examples
<p><b>Simple fistula:</b> Appears as an extra-enteric tract, with or without internal air or fluid; affected loops are often angulated or tethered.</p> <p><b>Complex fistula:</b> Multiple tracts often forming an asterisk-shaped or 'clover-leaf' appearance, or 'star sign'; affected loops are often angulated or tethered.</p>	 <p>CT</p>  <p>MRI</p>  <p>Ultrasound</p>

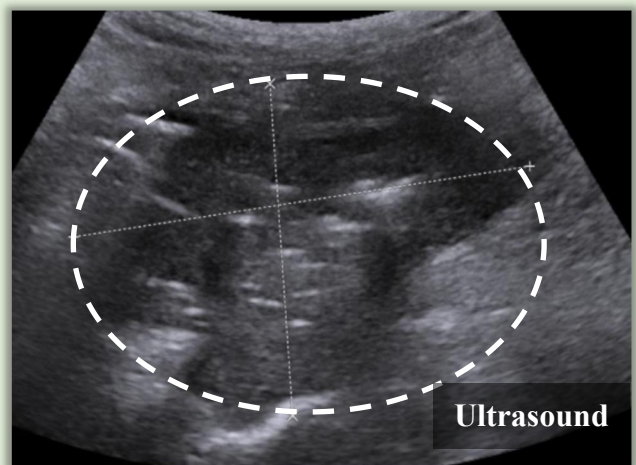
Penetrating disease<sup>1</sup>  
(Abscess and inflammatory mass)


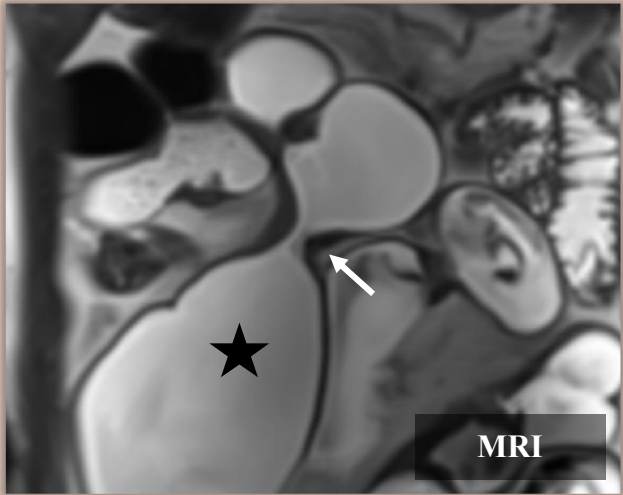
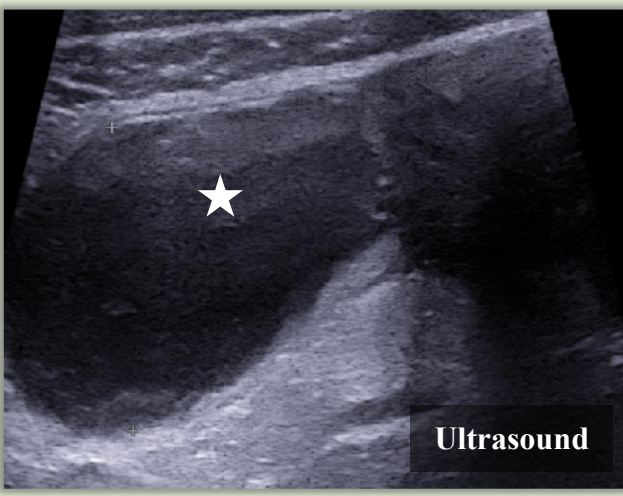
Examples



**Abscess:** Mesenteric or peritoneal fluid collection with rim enhancement and/or internal air.

**Inflammatory mass:** Ill-defined mass-like process of mixed fat and/or soft tissue attenuation/signal intensity.



Bowel stricture with upstream dilatation <sup>2</sup>	Examples
<p><b>Combination of the following criteria:</b></p> <p>(1) Localised luminal narrowing (luminal diameter reduction by at least 50%, measured relative to a normal adjacent appropriately distended bowel loop);</p> <p>(2) bowel wall thickening (increase in wall thickness of 25% in the maximally thickened area in an appropriately distended lumen, measured relative to a normal, adjacent, appropriately distended bowel loop);</p> <p>(3) upstream dilation (bowel diameter is 20% greater than the normal diameter in an appropriately distended lumen).</p> <p>✚ Bowel stricture (↑)</p> <p>✚ Upstream dilation (★)</p>	 <p>CT</p>  <p>MRI</p>  <p>Ultrasound</p>

1 Bruining DH, Zimmermann EM, Loftus Jr EV, et al. Consensus recommendations for evaluation, interpretation, and utilization of computed tomography and magnetic resonance enterography in patients with small bowel Crohn's disease. *Gastroenterology* 2018; **154**(4): 1172-94.

2 Rieder F, Bettenworth D, Ma C, et al. An expert consensus to standardise definitions, diagnosis and treatment targets for anti-fibrotic stricture therapies in Crohn's disease. *Alimentary pharmacology & therapeutics* 2018; **48**(3): 347-57.

**Supplementary Table. 2****R packages used in this study**

<b>Statistical analysis</b>	<b>R package</b>
Time-dependent ROC curves	timeROC
Hosmer-Lemeshow test	ResourceSelection
Net reclassification improvement (NRI) discrimination improvement (IDI)	PredictABEL
Unsupervised hierarchical clustering heatmap	pheatmap
Kaplan-Meier curves	ggsurvplot
Cox regression analysis	survival

**Supplementary Table. 3****Inter-/intra-observer reproducibility of extracted VAT and SAT radiomics features**

	<b>Interclass correlation coefficient</b>		<b>Intraclass correlation coefficient</b>	
	<b>Median</b>	<b>IQR</b>	<b>Median</b>	<b>IQR</b>
VAT radiomics features	1·000	0·998-1·000	1·000	0·999-1·000
SAT radiomics features	1·000	0·998-1·000	1·000	0·999-1·000

IQR, interquartile range; VAT, visceral adipose tissue; SAT, subcutaneous adipose tissue

**Supplementary Table. 4**

**The differences of the 36 selected VAT radiomics features between patients with and without disease progression**

Selected features	Training cohort (n=156)			Total test cohort (n=100)		
	Disease progression (n=28)	Non-Disease progression (n=128)	<i>P</i> value	Disease progression (n=16)	Non-Disease progression (n=84)	<i>P</i> value
original_shape_Flatness	0.352 (0.271, 0.480)	0.287 (0.177, 0.386)	0.074	0.476 (0.189, 0.565)	0.579 (0.455, 0.678)	0.009
original_shape_Maximum2DDiameter Column	0.220 (0.161, 0.270)	0.233 (0.179, 0.296)	0.220	0.397 (0.222, 0.584)	0.379 (0.244, 0.603)	0.981
original_shape_Maximum2DDiameter Row	0.221 (0.164, 0.287)	0.244 (0.178, 0.301)	0.282	0.458 (0.291, 0.701)	0.374 (0.293, 0.475)	0.090
original_firstorder_Maximum	0.121 (0.099, 0.345)	0.216 (0.105, 0.416)	0.120	0.124 (0.022, 0.741)	0.485 (0.323, 0.700)	0.023
original_glcM_InverseVariance	0.498 (0.309, 0.649)	0.610 (0.519, 0.695)	0.003	0.838 (0.641, 0.942)	0.845 (0.677, 0.952)	0.789
original_glcM_MaximumProbability	0.349 (0.245, 0.484)	0.281 (0.208, 0.374)	0.044	0.189 (0.095, 0.351)	0.137 (0.070, 0.247)	0.174
original_glszm_GrayLevelNonUnifor mityNormalized	0.338 (0.199, 0.497)	0.294 (0.180, 0.490)	0.461	0.509 (0.39, 0.764)	0.427 (0.368, 0.540)	0.041
original_gldm_LargeDependenceLow GrayLevelEmphasis	0.269 (0.133, 0.549)	0.177 (0.017, 0.400)	0.019	0.004 (0.002, 0.123)	0.003 (0.002, 0.005)	0.369
wavelet-LLH_glcM_Idn	0.841 (0.696, 0.948)	0.861 (0.734, 0.916)	0.816	0.824 (0.715, 0.882)	0.722 (0.517, 0.809)	0.000
wavelet-LLH_glszm_SmallAreaHigh GrayLevelEmphasis	0.526 (0.174, 0.640)	0.484 (0.304, 0.654)	0.720	0.010 (0.002, 0.071)	0.001 (0.000, 0.002)	0.000
wavelet-LLH_glszm_ZoneEntropy	0.685 (0.623, 0.786)	0.667 (0.542, 0.759)	0.359	0.476 (0.383, 0.580)	0.324 (0.177, 0.433)	0.001
wavelet-LHL_firstorder_Maximum	0.277 (0.136, 0.353)	0.260 (0.162, 0.373)	0.834	0.156 (0.067, 0.348)	0.355 (0.280, 0.420)	0.001
wavelet-LHH_glrM_GrayLevelNonU niformityNormalized	0.900 (0.811, 0.921)	0.842 (0.721, 0.908)	0.028	0.976 (0.941, 0.981)	0.992 (0.981, 0.992)	0.000



wavelet-LHH_gldm_DependenceVariance	0.650 (0.457, 0.743)	0.649 (0.532, 0.742)	0.428	0.478 (0.318, 0.620)	0.574 (0.463, 0.790)	0.004
wavelet-HLL_firstorder_Kurtosis	0.209 (0.094, 0.363)	0.240 (0.133, 0.385)	0.340	0.047 (0.031, 0.078)	0.063 (0.036, 0.102)	0.257
wavelet-HLL_glcm_Idn	0.889 (0.788, 0.935)	0.891 (0.843, 0.930)	0.816	0.465 (0.38, 0.544)	0.505 (0.340, 0.594)	0.257
wavelet-HLL_glszm_LargeAreaLowGrayLevelEmphasis	0.016 (0.001, 0.106)	0.003 (0.001, 0.028)	0.091	0.000 (0.000, 0.009)	0.000 (0.000, 0.001)	0.065
wavelet-HLH_glcm_MCC	0.519 (0.345, 0.630)	0.440 (0.340, 0.537)	0.850	0.639 (0.472, 0.736)	0.287 (0.035, 0.506)	0.000
wavelet-HLH_glrln_HighGrayLevelRunEmphasis	0.110 (0.048, 0.336)	0.192 (0.086, 0.423)	0.208	0.067 (0.024, 0.167)	0.017 (0.000, 0.043)	0.002
wavelet-HLH_glszm_LargeAreaLowGrayLevelEmphasis	0.002 (0.000, 0.009)	0.000 (0.000, 0.006)	0.101	0.000 (0.000, 0.004)	0.002 (0.000, 0.014)	0.047
wavelet-HLH_glszm_SmallAreaHighGrayLevelEmphasis	0.108 (0.041, 0.332)	0.158 (0.076, 0.356)	0.215	0.044 (0.023, 0.157)	0.009 (0.001, 0.024)	0.000
wavelet-HLH_gldm_SmallDependenceLowGrayLevelEmphasis	0.102 (0.014, 0.186)	0.058 (0.022, 0.159)	0.727	0.012 (0.006, 0.043)	0.053 (0.018, 0.286)	0.001
wavelet-HHL_firstorder_Maximum	0.304 (0.178, 0.452)	0.366 (0.254, 0.493)	0.085	0.063 (0.020, 0.283)	0.245 (0.133, 0.358)	0.002
wavelet-HHL_glszm_GrayLevelNonUniformityNormalized	0.495 (0.165, 0.630)	0.284 (0.131, 0.476)	0.057	0.360 (0.094, 0.684)	0.146 (0.074, 0.277)	0.019
wavelet-HHH_firstorder_Maximum	0.351 (0.280, 0.531)	0.382 (0.285, 0.491)	0.623	0.263 (0.196, 0.323)	0.144 (0.039, 0.249)	0.001
wavelet-LLL_gldm_LargeDependenceLowGrayLevelEmphasis	0.268 (0.051, 0.453)	0.123 (0.015, 0.282)	0.014	0.003 (0.001, 0.206)	0.003 (0.002, 0.004)	0.472
log-sigma-1-0-mm-3D_firstorder_InterquartileRange	0.306 (0.259, 0.434)	0.432 (0.304, 0.554)	0.010	0.612 (0.312, 0.729)	0.633 (0.429, 0.791)	0.199
log-sigma-1-0-mm-3D_firstorder_Maximum	0.269 (0.149, 0.369)	0.264 (0.170, 0.383)	0.603	0.198 (0.122, 0.263)	0.195 (0.151, 0.237)	0.899

log-sigma-1-0-mm-3D_glrml_LongRunLowGrayLevelEmphasis	0.059 (0.035, 0.078)	0.038 (0.023, 0.058)	0.027	0.044 (0.012, 0.117)	0.026 (0.011, 0.073)	0.216
log-sigma-3-0-mm-3D_firstorder_Maximum	0.228 (0.144, 0.324)	0.230 (0.179, 0.349)	0.367	0.347 (0.234, 0.508)	0.374 (0.301, 0.505)	0.608
log-sigma-3-0-mm-3D_glcml_ClusterProminence	0.030 (0.017, 0.111)	0.060 (0.032, 0.125)	0.118	0.012 (0.007, 0.031)	0.015 (0.008, 0.030)	0.490
log-sigma-3-0-mm-3D_glcml_DifferenceVariance	0.285 (0.170, 0.491)	0.396 (0.260, 0.534)	0.028	0.269 (0.135, 0.332)	0.249 (0.196, 0.345)	0.411
log-sigma-5-0-mm-3D_glcml_JointEnergy	0.400 (0.282, 0.574)	0.283 (0.189, 0.449)	0.036	0.364 (0.238, 0.492)	0.398 (0.254, 0.540)	0.695
log-sigma-5-0-mm-3D_glrml_LowGrayLevelRunEmphasis	0.203 (0.138, 0.358)	0.216 (0.156, 0.310)	0.673	0.266 (0.203, 0.359)	0.295 (0.178, 0.421)	0.699
log-sigma-5-0-mm-3D_glszm_GrayLevelNonUniformityNormalized	0.370 (0.222, 0.466)	0.316 (0.197, 0.450)	0.461	0.336 (0.192, 0.730)	0.309 (0.151, 0.460)	0.220
log-sigma-5-0-mm-3D_gldml_DependenceVariance	0.801 (0.596, 0.843)	0.673 (0.525, 0.798)	0.019	0.457 (0.408, 0.584)	0.510 (0.383, 0.636)	0.582

VAT, visceral adipose tissue. Data are presented as the median (interquartile range) of the selected features in the training and total test cohorts. An independent t-test or the Mann-Whitney U test was performed to assess the differences of the features between disease progression and non-disease progression.

Note. The radiomics features selection method in this study determines that the selected radiomics features are not necessary to have a linear difference between disease progression and non-disease progression.

Supplementary Table. 5

## Prediction performance of VAT-RM and SAT-RM in different CT scanners

CT scanners	AUC (95% CI)	Sensitivity	Specificity	Accuracy	<i>P</i> value
<b>VAT-RM</b>					
<b>Training cohort</b>					
No.1	0.836 (0.740, 0.908)	0.733	0.971	0.929	<0.001
No.2	0.916 (0.756, 0.986)	0.857	0.957	0.933	<0.001
No.3	0.881 (0.742, 0.961)	0.667	0.971	0.927	<0.001
<b>Test cohort</b>					
No.4	0.820 (0.687, 0.914)	0.889	0.667	0.706	<0.001
No.5	0.871 (0.744, 0.949)	0.714	1.000	0.959	<0.001
<b>SAT-RM</b>					
<b>Training cohort</b>					
No.1	0.855 (0.762, 0.922)	0.533	0.957	0.882	<0.001
No.2	0.870 (0.696, 0.964)	0.429	1.000	0.867	<0.001
No.3	0.900 (0.766, 0.971)	0.833	0.800	0.805	<0.001
<b>Test cohort</b>					
No.4	0.741 (0.599, 0.853)	0.778	0.714	0.725	0.022
No.5	0.803 (0.664, 0.903)	0.571	1.000	0.939	0.017

AUC, area under ROC curve; CI, confidence interval; VAT, visceral adipose tissue; SAT, subcutaneous adipose tissue; RM, radiomics model.

*P*-value is the significance level of the comparison of the area under the receiver operating characteristic curve (AUC) with that of a random case (AUC = 0.500).

**Supplementary Table. 6**

**Comparisons with AUC of radiomics models among five CT scanners using DeLong test**

CT scanners	No.1	No.2	No.3	No.4	No.5
No.1		0.440	0.701	0.867	0.775
No.2	0.893		0.773	0.348	0.719
No.3	0.623	0.795		0.599	0.941
No.4	0.332	0.354	0.212		0.673
No.5	0.704	0.670	0.508	0.707	

The upper right part of the table (Gray background) shows the *P*-values for the VAT-RM in different CT scanners. The bottom left part of the table (Blue background) shows the *P*-values for the SAT-RM in different CT scanners.

AUC, area under ROC curve; CI, confidence interval; VAT, visceral adipose tissue; SAT, subcutaneous adipose tissue; RM, radiomics model.

*P*-value is the significance level of the comparison of the area under the receiver operating characteristic curve (AUC) with that of a random case (AUC = 0.500).

**Supplementary Table. 7**

**The differences of the 35 selected SAT radiomics features between patients with and without disease progression**

Selected features	Training cohort (n=156)			Total test cohort (n=100)		
	Disease progression (n=28)	Non-Disease progression (n=128)	<i>P</i> value	Disease progression (n=16)	Non-Disease progression (n=84)	<i>P</i> value
original_shape_MinorAxisLength	0.713 (0.638, 0.820)	0.749 (0.633, 0.839)	0.242	0.854 (0.808, 0.922)	0.766 (0.643, 0.848)	0.002
original_firstorder_Skewness	0.620 (0.433, 0.819)	0.573 (0.412, 0.682)	0.123	0.855 (0.825, 0.880)	0.856 (0.826, 0.880)	0.884
original_glrlm_RunVariance	0.217 (0.096, 0.279)	0.152 (0.070, 0.234)	0.103	0.022 (0.011, 0.030)	0.055 (0.013, 0.153)	0.037
original_gldm_DependenceEntropy	0.663 (0.521, 0.756)	0.686 (0.594, 0.756)	0.487	0.852 (0.711, 0.887)	0.748 (0.607, 0.849)	0.045
wavelet-LLH_glcM_MCC	0.575 (0.483, 0.694)	0.599 (0.418, 0.700)	0.921	0.664 (0.507, 0.787)	0.325 (0.176, 0.501)	0.000
wavelet-LLH_glszm_GrayLevelNonUniformityNormalized	0.593 (0.439, 0.754)	0.557 (0.452, 0.699)	0.333	0.648 (0.126, 0.730)	0.782 (0.727, 0.851)	0.000
wavelet-LHL_firstorder_10Percentile	0.467 (0.251, 0.647)	0.337 (0.197, 0.449)	0.010	0.537 (0.412, 0.767)	0.692 (0.405, 0.848)	0.330
wavelet-LHL_gldm_SmallDependenceHighGrayLevelEmphasis	0.045 (0.015, 0.133)	0.039 (0.019, 0.095)	0.947	0.157 (0.070, 0.365)	0.136 (0.061, 0.220)	0.190
wavelet-LHH_glcM_Imc1	0.726 (0.689, 0.823)	0.761 (0.651, 0.822)	0.917	0.581 (0.464, 0.974)	0.672 (0.396, 0.946)	0.635
wavelet-LHH_glszm_GrayLevelNonUniformityNormalized	0.771 (0.543, 0.933)	0.698 (0.366, 0.881)	0.162	0.825 (0.566, 0.834)	0.835 (0.834, 0.848)	0.000
wavelet-LHH_glszm_GrayLevelVariance	0.073 (0.019, 0.146)	0.098 (0.041, 0.221)	0.149	0.019 (0.015, 0.124)	0.015 (0.014, 0.015)	0.000
wavelet-LHH_glszm_SmallAreaLowGrayLevelEmphasis	0.109 (0.079, 0.320)	0.186 (0.088, 0.361)	0.065	0.211 (0.143, 0.781)	0.823 (0.690, 0.871)	0.000
wavelet-LHH_glszm_ZoneEntropy	0.597 (0.485, 0.724)	0.554 (0.474, 0.641)	0.130	0.461 (0.415, 0.554)	0.369 (0.223, 0.489)	0.015
wavelet-HLL_glcM_DifferenceEntropy	0.391 (0.143, 0.582)	0.496 (0.355, 0.746)	0.003	0.278 (0.181, 0.368)	0.165 (0.060, 0.343)	0.146

wavelet-HLL_glrml_ShortRunLowGrayLevelEmphasis	0.021 (0.005, 0.067)	0.049 (0.002, 0.257)	0.392	0.013 (0.002, 0.070)	0.032 (0.006, 0.072)	0.180
wavelet-HLL_glszm_GrayLevelVariance	0.053 (0.030, 0.116)	0.043 (0.027, 0.167)	0.895	0.050 (0.032, 0.106)	0.035 (0.018, 0.056)	0.163
wavelet-HLL_gldm_LargeDependenceHighGrayLevelEmphasis	0.054 (0.012, 0.138)	0.023 (0.004, 0.361)	0.412	0.018 (0.003, 0.095)	0.007 (0.002, 0.040)	0.209
wavelet-HLL_ngtdm_Strength	0.016 (0.005, 0.080)	0.033 (0.009, 0.102)	0.302	0.003 (0.001, 0.007)	0.001 (0.000, 0.004)	0.136
wavelet-HLH_glcm_Idn	0.734 (0.693, 0.790)	0.696 (0.587, 0.787)	0.063	0.564 (0.542, 0.897)	0.083 (0.032, 0.356)	0.000
wavelet-HLH_glcm_Imc1	0.697 (0.632, 0.756)	0.678 (0.581, 0.730)	0.101	0.658 (0.488, 0.928)	0.783 (0.507, 0.919)	1.000
wavelet-HHL_glcm_DifferenceEntropy	0.239 (0.079, 0.381)	0.303 (0.207, 0.464)	0.055	0.320 (0.193, 0.376)	0.210 (0.076, 0.544)	0.602
wavelet-HHH_firstorder_Median	0.596 (0.515, 0.641)	0.610 (0.569, 0.647)	0.309	0.690 (0.674, 0.713)	0.694 (0.673, 0.702)	0.862
wavelet-HHH_glszm_ZoneEntropy	0.353 (0.269, 0.430)	0.301 (0.232, 0.380)	0.123	0.470 (0.356, 0.555)	0.419 (0.243, 0.518)	0.120
wavelet-HHH_gldm_LowGrayLevelEmphasis	0.276 (0.276, 0.992)	0.276 (0.276, 0.991)	0.636	0.946 (0.164, 0.948)	0.947 (0.945, 0.949)	0.026
wavelet-LLL_glcm_InverseVariance	0.718 (0.557, 0.902)	0.839 (0.699, 0.912)	0.101	0.835 (0.790, 0.891)	0.697 (0.317, 0.865)	0.011
wavelet-LLL_glrml_LongRunLowGrayLevelEmphasis	0.291 (0.142, 0.536)	0.268 (0.118, 0.439)	0.255	0.012 (0.003, 0.023)	0.013 (0.005, 0.041)	0.374
log-sigma-1-0-mm-3D_firstorder_Maximum	0.320 (0.214, 0.539)	0.392 (0.291, 0.516)	0.081	0.591 (0.408, 0.741)	0.364 (0.223, 0.548)	0.001
log-sigma-1-0-mm-3D_firstorder_Skewness	0.511 (0.272, 0.706)	0.658 (0.297, 0.763)	0.110	0.669 (0.525, 0.810)	0.642 (0.526, 0.742)	0.611
log-sigma-1-0-mm-3D_glcm_SumSquares	0.180 (0.123, 0.299)	0.184 (0.119, 0.284)	0.969	0.082 (0.068, 0.108)	0.073 (0.050, 0.124)	0.395
log-sigma-1-0-mm-3D_glrml_RunVar	0.398 (0.199, 0.617)	0.364 (0.198, 0.486)	0.157	0.116 (0.089, 0.160)	0.255 (0.108, 0.519)	0.013

iance						
log-sigma-1-0-mm-3D_glszm_GrayLe	0.243 (0.142, 0.331)	0.295 (0.140, 0.472)	0.184	0.312 (0.150, 0.547)	0.154 (0.069, 0.285)	0.013
velNonUniformity						
log-sigma-3-0-mm-3D_firstorder_Kurt	0.148 (0.041, 0.519)	0.167 (0.070, 0.396)	0.783	0.028 (0.014, 0.070)	0.032 (0.013, 0.062)	0.789
osis						
log-sigma-5-0-mm-3D_gldm_Idm	0.318 (0.265, 0.374)	0.282 (0.212, 0.381)	0.220	0.301 (0.244, 0.338)	0.309 (0.248, 0.366)	0.589
log-sigma-5-0-mm-3D_gldm_LowGra	0.049 (0.023, 0.106)	0.084 (0.039, 0.152)	0.053	0.083 (0.055, 0.112)	0.137 (0.078, 0.255)	0.033
yLevelEmphasis						
log-sigma-5-0-mm-3D_ngtdm_Contra	0.119 (0.106, 0.222)	0.187 (0.116, 0.275)	0.038	0.236 (0.183, 0.353)	0.273 (0.187, 0.390)	0.321
st						

---

SAT, subcutaneous adipose tissue. Data are presented as the median (interquartile range) of the selected features in the training and total test cohorts. An independent t-test or the Mann-Whitney U test was performed to assess the differences of the features between disease progression and non-disease progression.

Note. The radiomics features selection method in this study determines that the selected radiomics features are not necessary to have a linear difference between disease progression and non-disease progression.

**Supplementary Table. 8**

**The differences of other adipose tissue metrics between CD patients with and without disease progression**

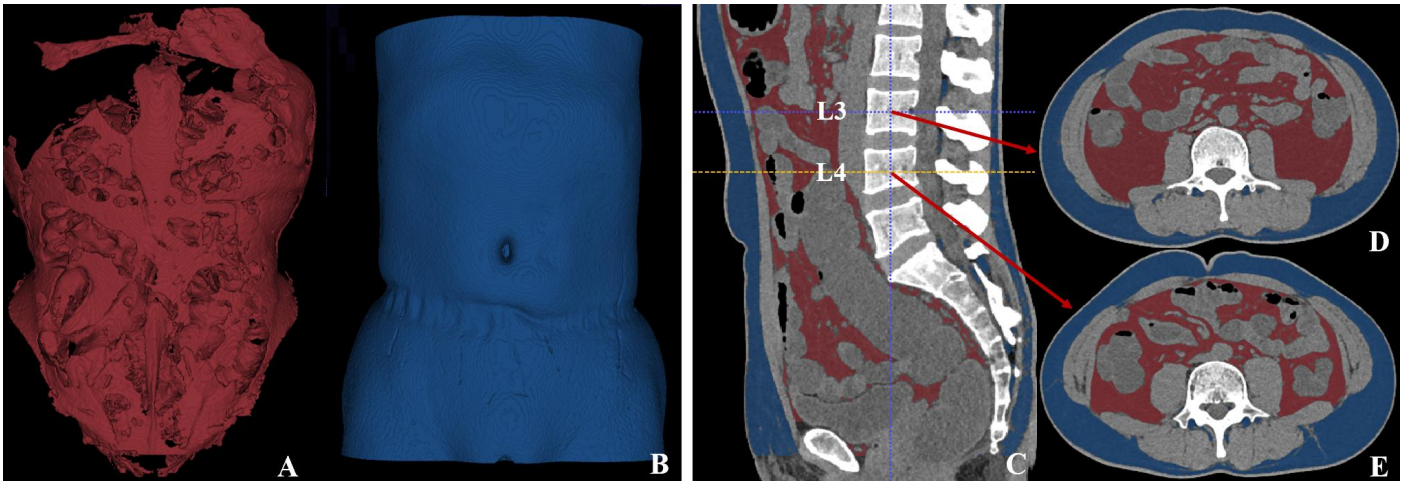
Metrics	Training cohort (n=156)			Total test cohort (n=100)		
	Disease progression (n=28)	Non-Disease progression (n=128)	<i>P</i> value	Disease progression (n=16)	Non-Disease progression (n=84)	<i>P</i> value
BMI (kg/m <sup>2</sup> )	17.699 (16.436, 20.202)	18.922 (17.110, 20.934)	0.089	18.687 (15.070, 21.675)	17.954 (15.606, 19.300)	0.304
VAT volume (×10 <sup>5</sup> mm <sup>3</sup> )	1.186 (0.637, 5.634)	0.957 (0.353, 3.464)	0.387	3.642 (1.516, 11.966)	5.084 (2.719, 10.160)	0.532
SAT volume (×10 <sup>5</sup> mm <sup>3</sup> )	6.056 (1.604, 10.916)	6.960 (1.326, 12.620)	0.841	5.346 (2.906, 12.954)	6.733 (1.342, 14.059)	0.825
VAT/SAT volume ratio	0.395 (0.216, 0.643)	0.291 (0.159, 0.562)	0.251	0.725 (0.340, 2.930)	1.127 (0.587, 3.098)	0.206
VAT/SAT area ratio at L3 level	0.932 (0.639, 1.154)	0.986 (0.709, 1.400)	0.102	1.040 (0.622, 1.438)	0.966 (0.580, 1.387)	0.532
VAT/SAT area ratio at L4 level	0.911 (0.733, 1.096)	0.906 (0.660, 1.225)	0.426	0.830 (0.687, 1.323)	0.861 (0.616, 1.334)	0.996

CD, Crohn's disease; BMI, body mass index; VAT, visceral adipose tissue; SAT, subcutaneous adipose tissue

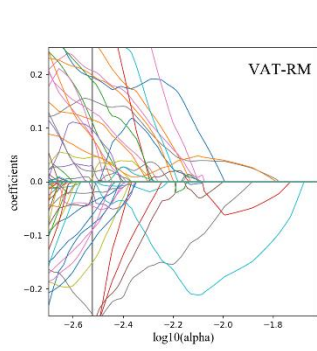
Non-normally distributed variables, expressed as median (interquartile range), line Mann-Whitney U test



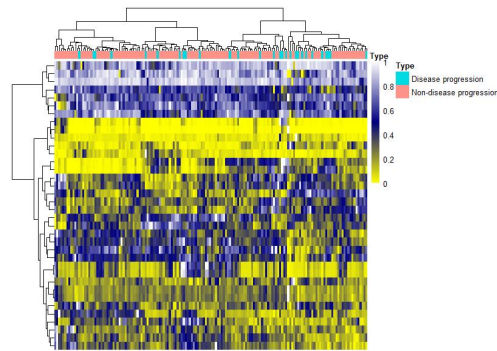
## Supplementary Figures



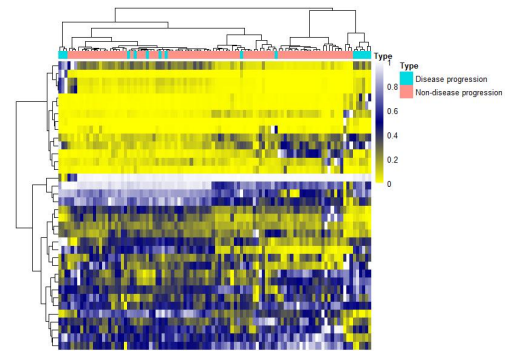
**Supplementary Figure 1.** The measurement of the five traditional fat metrics on CT images. VAT volume ( $\text{mm}^3$ ) was calculated using VOIs of VAT with the open-source pyradiomics toolkit mentioned in the main text (A). The calculation of SAT volume (B) was the same as that of VAT volume. VAT/SAT volume ratio is equal to VAT volume divided by SAT volume. After localisation of the lumbar vertebrae on sagittal CT (C), VAT and SAT areas on CT at the L3 (D) and L4 (E) vertebral level were automatically measured respectively, using the open-source opencv-python toolkit. VAT/SAT area ratios at the levels of L3 and L4 were equal to VAT area divided by SAT area. (CT, computerized tomography; VAT, visceral adipose tissue; VOI, Volume of interests; SAT, subcutaneous adipose tissue)



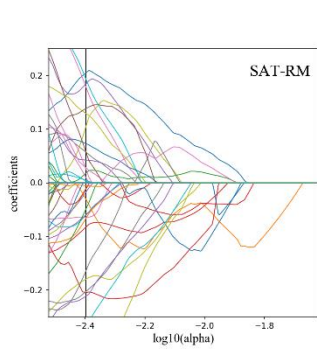
Supplementary figure 2A



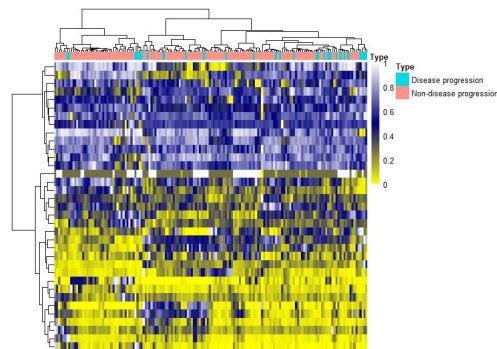
Supplementary figure 2B



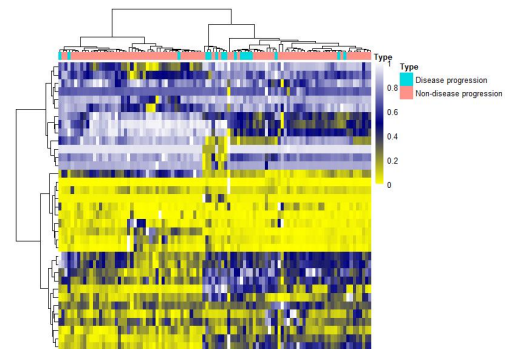
Supplementary figure 2C



Supplementary figure 2D



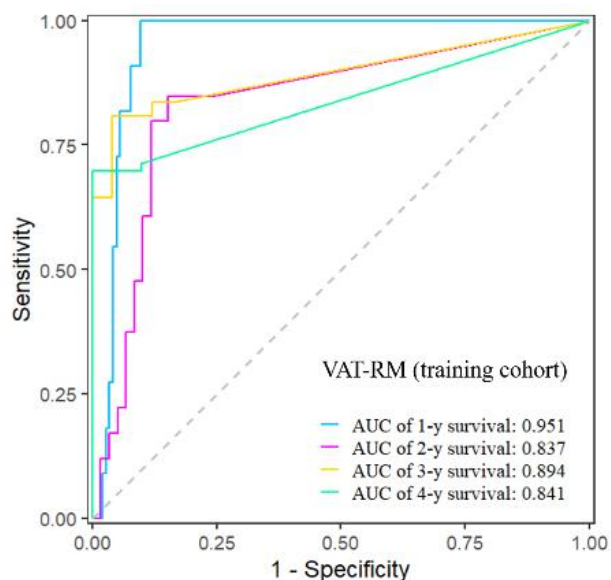
Supplementary figure 2E



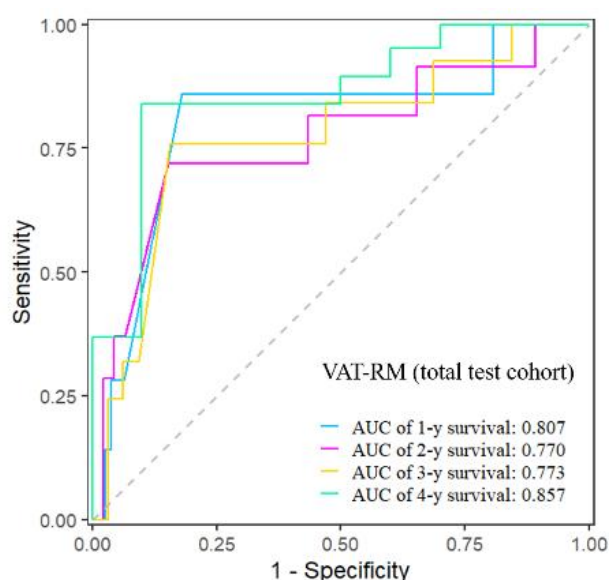
Supplementary figure 2F

**Supplementary Figure 2.** VAT radiomics feature selection using LASSO. (A) LASSO coefficient profiles of 1128 selected VAT radiomics features. A line was drawn at the optimal value of the  $\alpha$  parameter determined using a grid search method, which resulted in 36 features with non-zero coefficients. Heatmap generated by unsupervised hierarchical clustering of the selected features in the (B) training cohort and (C) total test cohort of VAT. To achieve a clear view, the feature expression has been normalised to the range 0–1. Each row in the heatmap is one selected radiomics feature with standardised feature values ( $n = 36$ ). The dendrogram at the top represents subgroups of disease progression with similar information determined by clustering. Similar to the radiomics features selection of VAT, (D) LASSO coefficient profiles of 1118 selected SAT radiomics features. A line was drawn at the optimal value of the  $\alpha$  parameter determined using a grid search method, which resulted in 35 features with non-zero coefficients. Heatmap generated by unsupervised hierarchical clustering of the selected features in the (E) training cohort and (F) total test cohort of SAT.

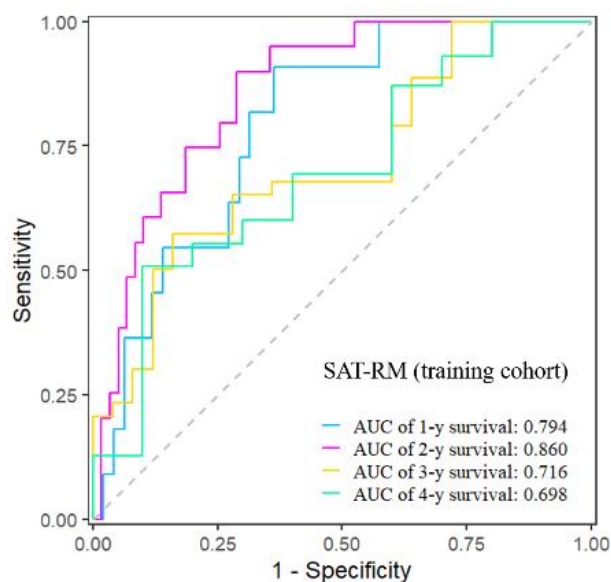
(VAT, visceral adipose tissue; SAT, subcutaneous adipose tissue; LASSO, least absolute shrinkage and selection operator)



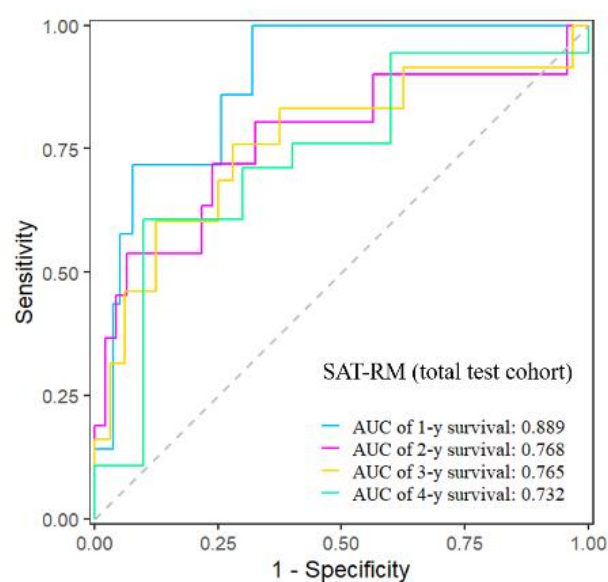
Supplementary figure 3A



Supplementary figure 3B



Supplementary figure 3C



Supplementary figure 3D

**Supplementary Figure 3.** Comparison of predictive performance between VAT-RM and SAT-RM using Time-dependent receiver operating characteristic curve analysis. Time-dependent receiver operating characteristic curve of disease progression-free survival at one, two, three, and four years for the VAT-RM in training cohort (A) and total test cohort (B), and for the SAT-RM in training cohort (C) and total test cohort (D), revealing higher AUCs of VAT-RM than that of SAT-RM at most of time points. (VAT, visceral adipose tissue; SAT, subcutaneous adipose tissue; RM, radiomics model; AUC, area under the receiver operating characteristic curve)